Angular dependence of the intensity of light beams diffracted by colloidal crystals

Gabriel Lozano,[1] Javier E. Mazzaferri,[2] Luis A. Dorado,[3] Silvia Ledesma,[2] Ricardo A. Depine,[3,4] and Hernán Míguez[1,*]

[1]*Instituto de Ciencia de Materiales de Sevilla, Consejo Superior de Investigaciones Científicas, Sevilla, Spain*
[2]*Laboratorio de Procesado de Imágenes, Departamento de Física, Facultad de Ciencias Exactas y Naturales, Universidad de Buenos Aires, Argentina*
[3]*Grupo de Electromagnetismo Aplicado, Departamento de Física, Facultad de Ciencias Exactas y Naturales, Universidad de Buenos Aires, Argentina*
[4]*E-mail: rdep@df.uba.ar*
[*]*Corresponding author: hernan@icmse.csic.es*

Received January 27, 2010; revised April 9, 2010; accepted April 27, 2010; posted April 30, 2010 (Doc. ID 123403); published June 17, 2010

An experimental and theoretical analysis of the angular dependence of the diffracted light beams emerging from three-dimensional colloidal photonic crystals is herein presented. Diffracted beams are identified according to their associated reciprocal-lattice vectors, and their intensities are obtained as a function of the zenithal and azimuthal incidence angles. Significant changes in the beam intensities are observed for large zenithal incidence angles as the azimuthal angle is varied. This phenomenon is related to the excitation of new resonant modes inside the photonic crystal which cannot be observed under normal incidence conditions. © 2010 Optical Society of America

OCIS codes: 050.1940, 050.5298, 050.6875, 160.4670, 160.4760.

1. INTRODUCTION

Since photonic crystals [1,2] were proposed as new materials to mold the flow of light two decades ago, they have attracted much attention in diverse fundamental and applied fields. Among all fabrication techniques developed up to date to prepare three-dimensional (3D) photonic crystals, those based on self-assembly are some of the most frequently employed and thoroughly analyzed [3,4]. The introduction of the evaporation induced self-assembly methods has largely improved the quality of the lattices [5,6] and made it possible to study for the first time fine optical phenomena [7–10]. In recent works, it has been reported that disorder in 3D photonic crystals dramatically affects the optical response in the so-called high-energy range, in which the lattice constant is equal or greater than the incident wavelength [11]. In fact, the origin of the fine features observed in this range has been the subject of an exciting debate [9,11–19]. It is precisely in this region where the most appealing phenomena occur. One of these is the optical diffraction. Although its observation was first reported and incipiently analyzed some years ago [13], the spectral dependence of the intensity of the diffracted beams emerging from a colloidal crystal remained unexplored. A full experimental and theoretical analysis of this has recently been reported for the case of normal incidence, that is, for an incident light beam perpendicular to the surface of a photonic crystal slab [20].

In this paper, we present a complete description of the angular dependence of light beams diffracted by 3D colloidal crystals, both theoretically and experimentally. We measured the relative intensity of each diffracted spot as both the zenithal and azimuthal incidence angles are varied when a laser beam impinges on a self-assembled 3D colloidal crystal. We use a Korringa–Kohn–Rostoker (KKR) approach to calculate the expected optical response of this kind of lattices. The effect of disorder is modeled by adding an imaginary part to the dielectric constant of the spheres [21], with a fairly precise reproduction of the experimental observations being attained. We report significant changes in the beam intensities for large zenithal incidence angles as the azimuthal angle is varied, which are explained in terms of the excitation of resonant modes inside the photonic crystal that cannot be observed under normal incidence conditions.

2. SAMPLE PREPARATION AND EXPERIMENTAL SETUP

Self-assembled 3D photonic crystal films were prepared as it is described in [4] by an evaporation induced self-assembly technique. In fact, the colloidal crystals were made by the deposition onto flat glass substrates of 750 nm polysterene spheres (IKERLAT, polydispersity below 3%, density of $\rho = 1.1\ \mathrm{g/cm^3}$, and refractive index of $n = 1.58$) suspended in water with particle volume fraction ranging from 0.05% to 0.20% and evaporated at temperatures ranging from 30°C to 60°C. As the suspension evaporates, a crystalline film is deposited on the substrate at the contact line with the suspension meniscus. The model structure is therefore a close-packed face-centered-cubic (FCC) lattice of spheres of dielectric constant $\varepsilon_s = 2.5 + i\varepsilon_i$, embedded in a medium of $\varepsilon_m = 1$, which would correspond to latex spheres in air. The imaginary part of the dielectric constant is introduced to account for

the presence of disorder in the structure [21] since the material the spheres are made of is transparent in the optical range analyzed [22]. Measurements have to be performed with the photonic crystal slab deposited on a glass substrate with a refractive index of 1.51, so this substrate is also included in the theoretical model.

In order to analyze the angular dependence of the fluctuations of the diffracted beams, we used the blue line (wavelength of $\lambda=473$ nm) of a solid state laser (Laserglow) as the light source. In the experiments performed, we varied the direction of the incident wavevector $\vec{k}_i$ with respect to the surface of the photonic crystal, whose exact crystalline orientation was known, both from the pattern of diffracted spots observed and the examination of its surface and cross section under the scanning electron microscope [4]. The experimental setup is drawn in Fig. 1(a). In this scheme, all relevant geometrical parameters are introduced. The relative orientation of the photonic crystal film with respect to the source and the screen or the detector is described using a Cartesian reference system as shown in Fig. 1(a). The laser beam is linearly polarized with the electric field vector always contained in the incidence plane (xz plane in our reference system). We analyzed the intensity of the diffracted beams for each incident zenithal angle (θ_i), varying the incident azimuthal angle (ϕ_i). The former is defined as the angle formed between the normal to the photonic crystal outer surface and the incident beam, which is parallel to the z axis in our reference system, while the latter is the angle formed between the longitudinal axis of the photonic crystal film [dotted line in Fig. 1(a)] and the incidence plane. The theoretical values of the zenithal and azimuthal angles were adjusted to those measured by fitting the positions of maxima and minima in the efficiency spectra and by knowing the crystalline orientation with respect to the supporting glass edges using a scanning electron microscope, as we mentioned. The colloidal crystal growth direction is indicated by the arrow tip drawn in the longitudinal axis in Fig. 1(a). The sample is mounted in two stages that allow rotations in the so defined zenithal and azimuthal directions. The longitudinal axis of the colloidal film coincides with the $(1,-1)$ direction of the surface lattice of the crystal, as described in Fig. 1(c), which is parallel to the x axis, for $\theta_i=0°$ and $\phi_i=0°$, in our reference system. In front of the crystal a diffusing screen is placed in such a way that its normal coincides with the direction of the specularly reflected channel. The spots on the screen were imaged by a lens on the charge-coupled device array of a camera (Sony XC-75), and the picture was digitalized and stored in a computer. The magnification of the imaging system was adjusted in order to obtain the highest quality image that contains all the diffracted orders to be measured. The set of acquired images was processed by digital image techniques to extract the information of the efficiency for the different angles of incidence; in all cases the azimuthal angle ϕ_i is varied from $-165°$ to $135°$ in steps of $5°$. The efficiency can be calculated by integrating the intensity in the corresponding spot area. Some further processing is necessary in order to reduce the noise background produced by the diffuse light. In our case we have used a threshold criterion. According to this, the efficiency of each nonspecular diffracted channel was calculated as the addition of all the pixels within each spot whose intensity values were above the assumed noise threshold. Furthermore, since efficiency of the specularly reflected beam was to be measured, too, the intensities of both the incoming and diffracted beam were measured using a silicon photodiode.

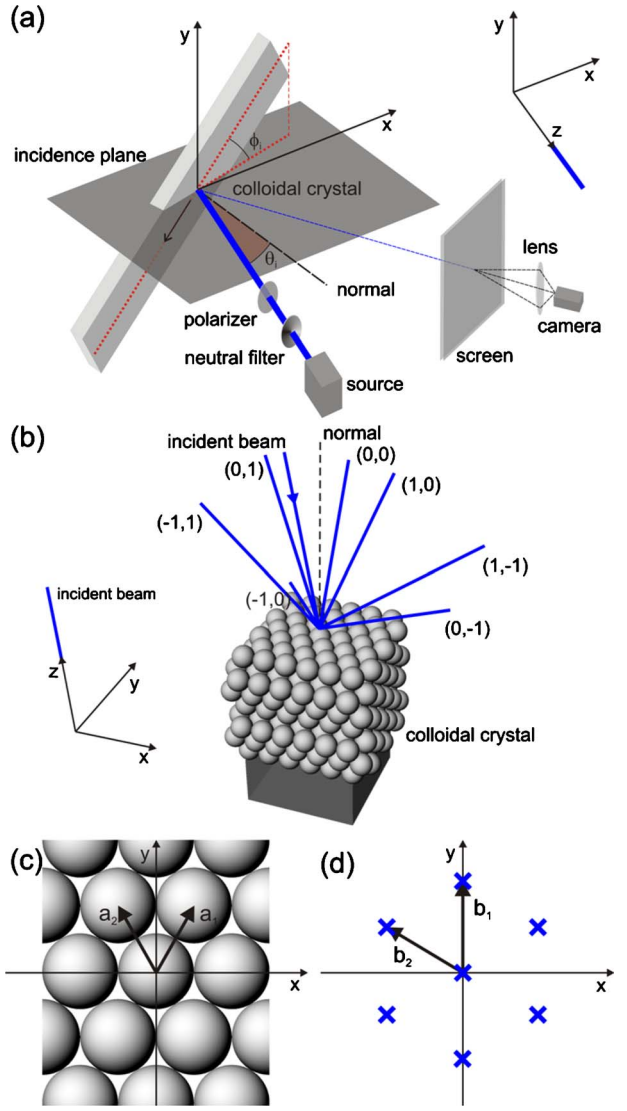

Fig. 1. (Color online) (a) Sketch of the experimental setup. (b) Scheme of the diffracted beams emerging from the colloidal crystal. Diagrams showing the two primitive vectors used to describe the (c) real and (d) reciprocal lattices.

Specular reflectance measurements were also performed at normal incidence for a wide range of wavelengths in order to precisely determine the crystal parameters from the fitting of the optical response. We used a Fourier transform infrared spectrophotometer (Bruker IFS-66) attached to a microscope. A 4× objective with a numerical aperture of 0.1 (light cone angle of 5.7°) was used to irradiate the lattices and collect the reflected light at quasinormal incidence with respect to its surface. This equipment allowed us to obtain absolute values for the specular reflectance at normal incidence, being straightforward the comparison between measured and calculated spectra.

3. DETERMINATION OF SIMULATION PARAMETERS

The intensities of diffracted beams were calculated using the vector KKR method in its layer version [23,24]. The crystal slab is first divided into layers parallel to a given crystallographic plane (111), with each layer containing a two dimensional (2D) lattice of identical spheres. A multipole expansion in vector spherical waves is used to calculate the multiple scattering in each 2D layer. Next, a plane wave expansion is used to calculate the multiple scattering between layers. In a numerical calculation, a maximum angular momentum L_{MAX} must be chosen in order to retain a finite number of terms in the series of spherical waves, while a maximum number of plane waves must also be defined. In all the calculations that follow, numerical convergence was obtained using a maximum value of the angular momentum $L_{MAX}=9$ in the spherical wave expansion and 41 plane waves. Since we are interested in FCC lattices and photonic crystal slabs with sphere layers piled up along the [111] direction, the spheres in each layer are ordered in a triangular lattice. If the sphere layers are parallel to the xy plane for $\theta_i=0°$ and $\phi_i=0°$, a set of 2D primitive lattice vectors is $\vec{a}_1=d(\hat{x}+\sqrt{3}\hat{y})/2$ and $\vec{a}_2=d(-\hat{x}+\sqrt{3}\hat{y})/2$, where d is the distance between spheres in the same layer [see Fig. 1(c)]. A set of primitive reciprocal-lattice vectors can be chosen as $\vec{b}_1=4\pi\hat{y}/(\sqrt{3}d)$ and $\vec{b}_2=2\pi(\hat{y}/\sqrt{3}-\hat{x})/d$ [see Fig. 1(d)], so any reciprocal-lattice vector can be written as $\vec{g}=p\vec{b}_1+q\vec{b}_2$, where (p,q) is a pair of integers. Since it is customary to use the lattice constant a of a classical cubic cell, we have $a=\sqrt{2}d$, so the photon energy is expressed in reduced units a/λ, where λ is the wavelength of the incident light.

The wavevector of a diffracted beam emerging from the slab can be written as $\vec{K}_{\vec{g}}^{\pm}=\vec{g}+\vec{k}_{i\|}\pm\sqrt{k^2-|\vec{g}+\vec{k}_{i\|}|^2}\hat{z}$, where the + (−) sign corresponds to a transmitted (reflected) beam [23], $\vec{k}_{i\|}$ is the component of the incident wavevector parallel to the surface of the slab (xy plane), $k=2\pi n_d/\lambda$, and n_d is the refractive index of the diffraction medium. Each diffracted beam corresponds to a propagating wave if the z-component of $\vec{K}_{\vec{g}}^{\pm}$ is purely real, so a diffraction channel $\vec{g}=p\vec{b}_1+q\vec{b}_2$ is open when $|\vec{g}+\vec{k}_{i\|}|<k$ and we have a diffraction cutoff whenever $|\vec{g}+\vec{k}_{i\|}|=k$. The efficiency of a diffraction channel (p,q) is denoted by $R_{(p,q)}$, so the total reflectance is given by $R=\Sigma_{(p,q)}R_{(p,q)}$ [11]. Therefore, $R_{(p,q)}$ is the relative intensity of the diffracted beam (p,q) and it is the parameter obtained in our measurements.

The calculated total reflectance spectrum of a colloidal crystal is shown in Fig. 2(a). As Checoury *et al.* reported, the different stacking patterns can be unambiguously identified by analyzing the optical response in the high-energy range [25]. Hence, the measurements presented in Fig. 2(b) correspond to the simulated spectrum of a FCC structure. Given the geometry of the lattice, we can calculate the diffraction cutoff as explained above, so we know that the opening of diffraction channels in air takes place at $a/\lambda=1.63$. Such a diffraction cutoff is indicated with a dashed line in Fig. 2(a). Specular reflectance measurements, presented in Fig. 2(b), were fitted using a code based on the vector KKR method [11]. From the optimum fitting [see Fig. 2(b)], the crystal thickness (seven layers) and the ε_i value (0.13) [26], related to the amount of disorder [21], were extracted. In order to fit the complete specular reflectance spectrum it is necessary to consider that the interparticle distance of actual colloidal crystals coincides with the expected diameter for spheres belonging to the same close-packed (111) plane but differs significantly in directions oblique to the [111] one. This leap has something to do with the fact that the spheres flatten along directions oblique to the normal to the substrate they are deposited on [27]. We find an excellent agreement between the theoretically simulated and the measured reflectance spectra. The lattice parameters (film thickness, lattice constants, or dielectric constants) obtained from this fitting are used in all ulterior calculations performed to analyze the efficiency of diffracted beams showed in next sections.

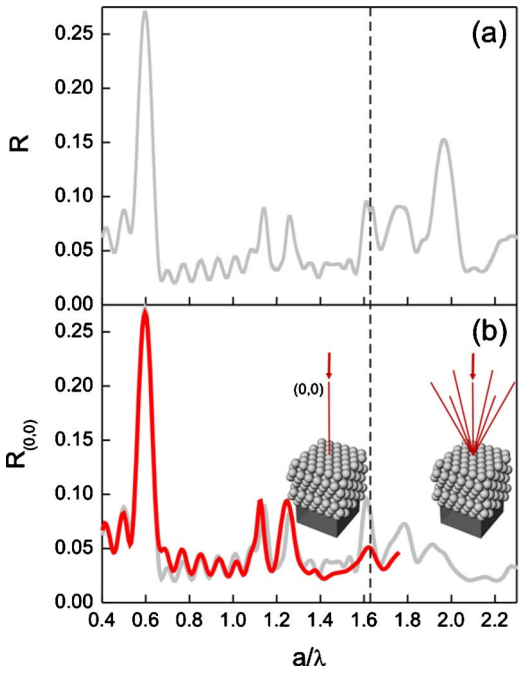

Fig. 2. (Color online) (a) Calculated total reflectance spectrum. (b) Measured (red thick line) and calculated (gray thin line) specular reflectance spectra. Vertical dashed line indicates the onset of diffraction for reflected modes.

4. IDENTIFICATION OF DIFFRACTED CHANNELS

Photographs of different diffraction patterns of reflected beams projected on a screen parallel to the xy plane taken when the blue laser impinges perpendicularly (zenithal angle of $\theta_i=0°$) onto the outer (111) plane of the colloidal crystal are shown in Fig. 3(a). Notice that the energy of the incident beam, in reduced units, is $a/\lambda=2.23$, well above the predicted cutoff at $a/\lambda=1.63$. Figure 3(b) shows diffracted spot patterns observed at the incident zenithal angle of $\theta_i=5°$. For both zenithal angles, the series of pictures illustrate the evolution of the diffraction pattern as the azimuthal angle increases.

The surface of the sample presents a triangular lattice structure with C_6 symmetry and subsequent layers are

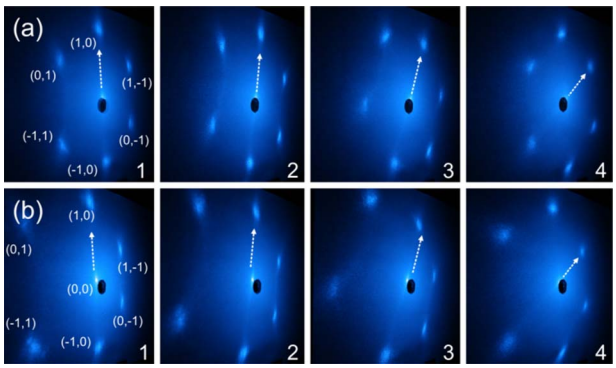

Fig. 3. (Color online) (a) Diffraction patterns of reflected beams projected on a screen parallel to the xy plane, when light illuminates the slab at (a) $\theta_i=0°$ and (b) $\theta_i=5°$. Photographs 1–4 correspond to the azimuthal angles $\phi_i=0°$, 15°, 30°, and 60°, respectively. Each spot is labeled according to its associated reciprocal-lattice vector. In all cases the arrow points at the (1,0) mode. The wavelength of the blue laser is 473 nm.

ordered following the well-known *ABCABC*… sequence, so diffraction pattern must show actually six spots with C_3 symmetry as it is described in [28,29]. In the case of normal incidence, the specularly reflected beam passes through the hole perforated in the screen to allow the laser illuminating the photonic crystal. The set of reciprocal-lattice vectors $\vec{b}_1$ and $\vec{b}_2$, shown in Fig. 1(d), is used to label this first set of diffracted beams as indicated in Fig. 3(a). The spots associated with these modes rotate with the sample. An arrow pointing at the (1,0) diffraction spot is plotted in each picture to easily follow the changes introduced by varying the azimuthal incident angle. In the clockwise direction, the other diffracted modes are identified as (1,−1), (0,−1), (−1,0), (−1,1), and (0,1).

Since the diffracted wavevector $\vec{K}_{\vec{g}}^{\pm}$ depends on the component of the incident wavevector parallel to the surface of the slab, the angular distribution of diffracted beams depends strongly on the tilt and rotation of the sample with respect to the incident beam. Also, just by looking at the two series of pictures shown in Fig. 3, it can be seen that the spot intensity $R_{(p,q)}$ fluctuates as the azimuthal angle is varied. This phenomenon is the subject of the next section.

5. ANALYSIS OF DIFFRACTED INTENSITY

Let us first analyze the dependence of the intensity of the specularly reflected beam as we vary the relative orientation of the photonic lattice with respect to the incident electric field. This diffracted channel, which we label as (0,0), forms an angle θ_d that is equal to the incident beam angle θ_i. This can be deduced by calculating $\vec{K}_{\vec{g}}^{\pm}$ for $\vec{g}=0$. When the azimuthal angle is varied, the (0,0) mode keeps its angular position constant but, interestingly, not its efficiency $R_{(0,0)}$. This is shown in Fig. 4, in which we plot both the measured (blue squares) and the calculated (gray line) intensity variations of the (0,0) mode as we change ϕ_i. Fair agreement between theory and experiment is found. The typical intensity variations as the azimuthal angle is modified are just a few percents in this case. Such intensity oscillations will be considerably more pronounced for the rest of diffraction modes, as we

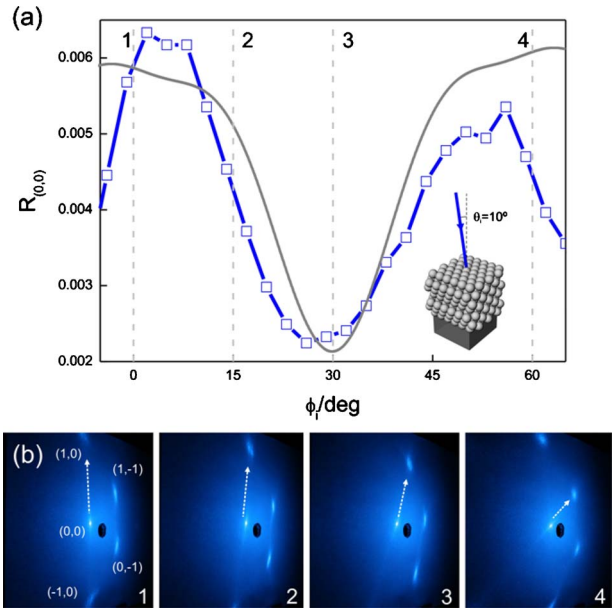

Fig. 4. (Color online) (a) Measured (blue squares) and calculated (gray line) reflection efficiencies of the diffracted channel (0,0) when the photonic crystal is illuminated at $\theta_i=10°$ and the azimuthal angle (ϕ_i) is varied. (b) Diffraction patterns of reflected beams. Photographs 1–4 correspond to the azimuthal angles $\phi_i=0°$, 15°, 30°, and 60°, respectively. Each spot is labeled according to its associated reciprocal-lattice vector. The arrow is always pointing at the (1,0) mode. The wavelength of the blue laser is 473 nm. Dashed vertical lines in (a) indicate the azimuthal angles at which the photographs in (b) were taken. The connecting solid blue line in (a) is only a guide for the eye.

present in this section. Figure 4(b) shows some of the images taken at different azimuthal angles used to obtain the data plotted in Fig. 4(a).

Although there is no angular or energy restriction for the propagation of the diffracted wave (i.e., the diffracted channel is open), the reflectance strongly varies and can even be zero (i.e., the mode is switched off). This cannot be explained using momentum transfer equations, but should be attributed to electromagnetic resonances occurring within the ordered array [30]. We select the diffracted channel (1,−1) to illustrate the dependence of the diffracted intensity with zenithal and azimuthal angle variations. In these experiments, the azimuthal angle is varied for two different zenithal angle illuminations, namely, $\theta_i=30°$ and 50°. In Fig. 5(a), we show the results of the measurements (blue squares) and calculations (gray line) of, respectively, the intensity and the reflection efficiency of the diffracted channel (1,−1), when the blue laser impinges at $\theta_i=30°$ and the photonic crystal slab is rotated from $\phi_i=-42°$ to 103°. Experimental data are obtained from the image processing, whereas the theoretical ones are obtained using the parameters extracted from the fitting shown in Fig. 2(b). Figure 5(b) shows in detail three of the images acquired for this analysis performed at $\theta_i=30°$. Only the (1,−1) mode is colored proportionally to its intensity for the sake of clarity. Images 1, 2, and 3 correspond to angular positions for which the intensity of this diffracted channel reaches a minimum, a maximum, and a minimum again, respectively. This behavior was also confirmed for other incident zenithal angles. In Fig. 6(a), we show the measured intensity (blue squares) and

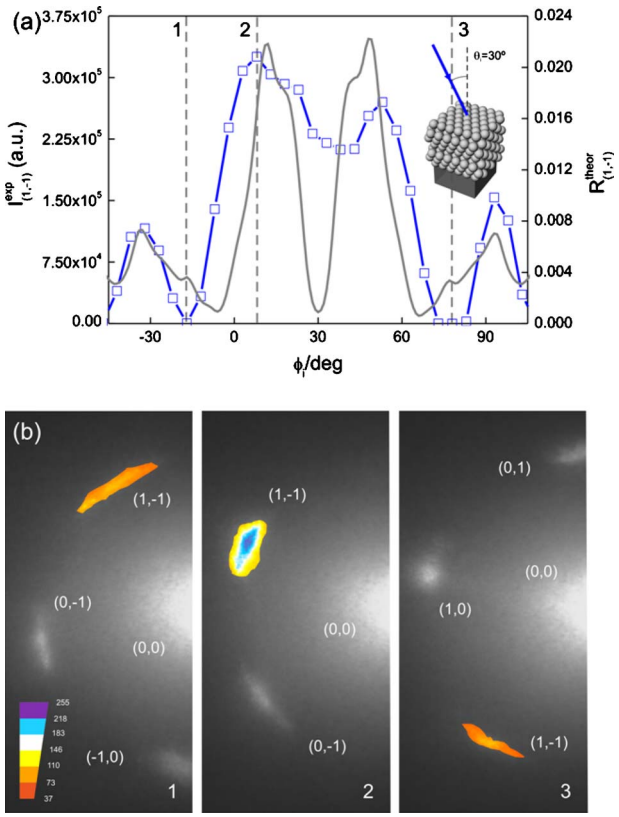

Fig. 5. (Color online) (a) Measured intensity (blue squares) and calculated reflection efficiency (gray line) of the diffracted channel $(1,-1)$ when the photonic crystal is illuminated at $\theta_i=30°$ and the azimuthal angle (ϕ_i) is varied. (b) Images of the emerged diffracted beams at $\phi_i=-17°$ (1), 8° (2), and 78° (3); the $(1,-1)$ mode is artificially colored to highlight its intensity. All the spots are labeled according to their associated reciprocal-lattice vectors. Intensity color scale is also indicated. Dashed vertical lines in (a) indicate the azimuthal angles at which the images in (b) were obtained. The connecting solid blue line in (a) is only a guide for the eye.

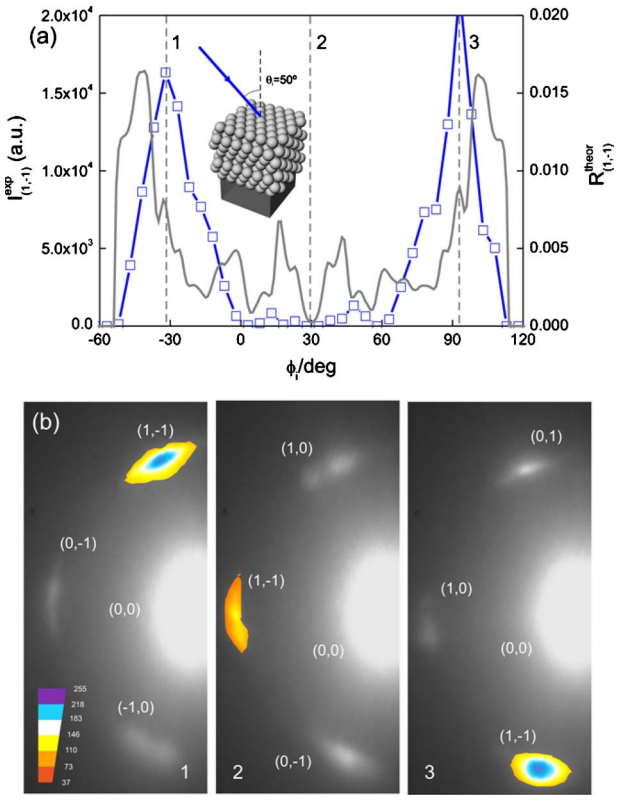

Fig. 6. (Color online) (a) Measured intensity (blue squares) and calculated reflection efficiency (gray line) of the diffracted channel $(1,-1)$ when the photonic crystal is illuminated at $\theta_i=50°$ and the azimuthal angle (ϕ_i) is varied. (b) Images of the emerged diffracted beams at $\phi_i=-32°$ (1), 33° (2), and 93° (3); the $(1,-1)$ mode is artificially colored to highlight its intensity. All the spots are labeled according to their associated reciprocal-lattice vectors. Intensity color scale is also indicated. Dashed vertical lines in (a) indicate the azimuthal angles at which the images in (b) were obtained. The connecting solid blue line in (a) is only a guide for the eye.

the theoretical reflection efficiency (gray line) of the same reflected diffracted channel $(1,-1)$, when the blue laser illuminates the slab at $\theta_i=50°$. In this case, the colloidal crystal is rotated from $\phi_i=-60°$ to 120°. Experimental data are obtained from the image processing, whereas the calculations are done using the parameters extracted from the fitting parameters obtained in Section 3. Again, good agreement between theory and experiment is found for the number of peaks, their positions, and relative intensities. Two minor peaks at azimuthal angles of 15° and 45° are obtained in the calculated efficiency curve, which cannot be observed in the measurements. As we mentioned in Section 2, the noise background produced by the diffuse light was reduced by using a threshold criterion and the efficiencies were calculated by integrating the measured beam intensity in the corresponding spot area. Unfortunately, this procedure for post-processing the measured data smoothed out the minor peaks observed in the calculated spectrum in Fig. 6(a). Figure 6(b) shows three of the acquired images for this zenithal angle taken at different azimuthal angles. It is possible to clearly identify two maxima, near $\phi_i\sim-30°$ and $\sim90°$ [see Fig. 6(b), panels 1 and 3], and observe that this channel is almost completely switched off at $\phi_i\sim30°$ [see Fig. 6(b), panel 2].

By comparing Fig. 5(a) ($\theta_i=30°$) and Fig. 6(a) ($\theta_i=50°$), we can see that the number of intensity peaks of channel $(1,-1)$ increases as the zenithal angle θ_i increases. We found that this phenomenon occurs regardless of the particular diffraction channel we are observing. In the case of normal incidence, it has been shown that peaks in the total reflectance as a function of the photon energy are due to the excitation of resonant modes inside the photonic crystal slab [30]. In this case, we can observe the appearance of resonances by analyzing the diffracted beam intensities as a function of the zenithal incidence angle. Therefore, for a constant photon energy above the diffraction cutoff, we can vary the zenithal and azimuthal angles of the incident beam in order to extract information about photonic resonant modes.

6. CONCLUSIONS

In summary, we have observed and measured the angular dependence of the reflection efficiency of modes diffracted by a colloidal crystal. Diffracted intensities have been measured as a function of both the incident zenithal and azimuthal angles. We have theoretically found the angular conditions at which diffracted modes are able to

emerge and propagate, as well as identified modes that switch off even though their respective diffracted channels are open. We have reproduced the features measured using the vector KKR method; good agreement between theory and experiments is found. We have observed an increment in the number of diffracted intensity peaks for large zenithal incidence angles, which occurs since new resonances are excited inside the photonic crystal slab. Therefore, we have presented an alternative method for analyzing resonances at a constant photon energy, which is a complementary approach to the study of reflectance as a function of energy at a constant incident beam direction.

ACKNOWLEDGMENTS

This research has been funded by the Spanish Ministry of Science and Innovation under grant MAT2007-02166 and Consolider HOPE CSD2007-00007, Junta de Andalucía under grant FQM3579, the Consejo Nacional de Investigaciones Científicas y Técnicas (CONICET, Argentina), and the Agencia Nacional de Promoción Científica y Tecnológica (PICT-11–1785). G. Lozano acknowledges the Consejo Superior de Investigaciones Cientificas (CSIC, Spain) for funding through an I3P scholarship.

REFERENCES AND NOTES

1. E. Yablonovitch, "Inhibited spontaneous emission in solid-state physics and electronics," Phys. Rev. Lett. **58**, 2059–2062 (1987).
2. S. John, "Strong localization of photons in certain disordered dielectric superlattices," Phys. Rev. Lett. **58**, 2486–2489 (1987).
3. C. López, "Three-dimensional photonic bandgap materials: semiconductors for light," J. Opt. A, Pure Appl. Opt. **8**, R1–R14 (2006).
4. G. Lozano, L. A. Dorado, R. A. Depine, and H. Míguez, "Towards a full understanding of the growth dynamics and optical response of self-assembled photonic colloidal crystal films," J. Mater. Chem. **19**, 185–190 (2009).
5. P. Jiang, J. F. Bertone, K. S. Hwang, and V. L. Colvin, "Single-crystal colloidal multilayers of controlled thickness," Chem. Mater. **11**, 2132–2140 (1999).
6. S. Wong, V. Kitaev, and G. A. Ozin, "Colloidal crystal films: advances in universality and perfection," J. Am. Chem. Soc. **125**, 15589–15598 (2003).
7. Y. A. Vlasov, X. Z. Bo, J. C. Sturm, and D. J. Norris, "On-chip natural assembly of silicon photonic bandgap crystals," Nature **414**, 289–293 (2001).
8. G. von Freymann, S. John, S. Wong, V. Kitaev, and G. A. Ozin, "Measurement of group velocity dispersion for finite size three-dimensional photonic crystals in the near-infrared spectral region," Appl. Phys. Lett. **86**, 053108 (2005).
9. H. Míguez, V. Kitaev, and G. Ozin, "Band spectroscopy of colloidal photonic crystal films," Appl. Phys. Lett. **84**, 1239–1241 (2004).
10. J. F. Galisteo-López, M. Galli, L. C. Andreani, A. Mihi, R. Pozas, M. Ocaña, and H. Míguez, "Phase delay and group velocity determination at a planar defect state in three dimensional photonic crystals," Appl. Phys. Lett. **90**, 101113 (2007).
11. L. A. Dorado, R. A. Depine, and H. Míguez, "Effect of extinction on the high-energy optical response of photonic crystals," Phys. Rev. B **75**, 241101(R) (2007).
12. J. F. Galisteo-López and C. López, "High-energy optical response of artificial opals," Phys. Rev. B **70**, 035108 (2004).
13. F. García-Santamaría, J. F. Galisteo-López, P. V. Braun, and C. López, "Optical diffraction and high-energy features in three-dimensional photonic crystals," Phys. Rev. B **71**, 195112 (2005).
14. A. V. Baryshev, V. A. Kosobukin, K. B. Samusev, D. E. Usvyat, and M. F. Limonov, "Light diffraction from opal-based photonic crystals with growth-induced disorder: experiment and theory," Phys. Rev. B **73**, 205118 (2006).
15. A. Balestreri, L. C. Andreani, and M. Agio, "Optical properties and diffraction effects in opal photonic crystals," Phys. Rev. E **74**, 036603 (2006).
16. S. Schutzmann, I. Venditti, P. Prosposito, M. Casalboni, and M. V. Russo, "High-energy angle resolved reflection spectroscopy on three-dimensional photonic crystals of self-organized polymeric nanospheres," Opt. Express **16**, 897–907 (2008).
17. L. A. Dorado, R. A. Depine, and H. Míguez, "Comment on "Observation of higher-order diffraction features in self-assembled photonic crystals"," Phys. Rev. A **78**, 037801 (2008).
18. R. V. Nair and R. Vijaya, "Reply to "Comment on 'Observation of higher-order diffraction features in self-assembled photonic crystals'"," Phys. Rev. A **78**, 037802 (2008).
19. S. G. Romanov, M. Bardosova, I. M. Povey, M. E. Pemble, and C. M. Sotomayor Torres, "Understanding of transmission in the range of high-order photonic bands in thin opal film," Appl. Phys. Lett. **92**, 191106 (2008).
20. L. A. Dorado, R. A. Depine, D. Schinca, G. Lozano, and H. Míguez, "Experimental and theoretical analysis of the intensity of beams diffracted by three-dimensional photonic crystals," Phys. Rev. B **78**, 075102 (2008).
21. L. A. Dorado and R. A. Depine, "Modeling of disorder effects and optical extinction in three-dimensional photonic crystals," Phys. Rev. B **79**, 045124 (2009).
22. T. Inagaki, E. T. Arakawa, R. N. Hamm, and M. W. Williams, "Optical properties of polystyrene from the near-infrared to the x-ray region and convergence of optical sum rules," Phys. Rev. B **15**, 3243–3253 (1977).
23. N. Stefanou, V. Yannopapas, and A. Modinos, "Heterostructures of photonic crystals: frequency bands and transmission coefficients," Comput. Phys. Commun. **113**, 49–77 (1998).
24. N. Stefanou, V. Yannopapas, and A. Modinos, "MULTEM 2: a new version of the program for transmission and band-structure calculations of photonic crystals," Comput. Phys. Commun. **132**, 189–196 (2000).
25. X. Checoury, S. Enoch, C. López, and A. Blanco, "Stacking patterns in self-assembly opal photonic crystals," Appl. Phys. Lett. **90**, 161131 (2007).
26. The imaginary part of the dielectric constant is not considered as a constant quantity during calculations. We employed a smaller value of the ε_i parameter in the high-energy spectral range (0.08) which represents the different effects of imperfections have on the different wavelength ranges.
27. G. Lozano, L. A. Dorado, D. Schinca, R. A. Depine, and H. Míguez, "Optical analysis of the fine crystalline structure of artificial opal films," Langmuir **25**, 12860–12864 (2009).
28. F. López-Tejeira, T. Ochiai, K. Sakoda, and J. Sánchez-Dehesa, "Symmetry characterization of eigenstates in opal-based photonic crystals," Phys. Rev. B **65**, 195110 (2002).
29. L. C. Andreani, A. Balestreri, J. F. Galisteo-López, M. Galli, M. Patrini, E. Descrovi, A. Chiodoni, F. Giorgis, L. Pallavidino, and F. Geobaldo, "Optical response with threefold symmetry axis on oriented microdomains of opal photonic crystals," Phys. Rev. B **78**, 205304 (2008).
30. L. A. Dorado, R. A. Depine, G. Lozano, and H. Míguez, "Physical origin of the high energy optical response of three dimensional photonic crystals," Opt. Express **15**, 17754–17760 (2007).